Data Fusion-based Method for the Assessment of Minimum Zone for Aspheric Optics

Zuowei Zhu[1] , Yassir Arezki[1,2] , Na Cai[1] , Charyar Mehdi-Souzani[1] , Nabil Anwer[1] and Hichem Nouira[2]

[1]LURPA, ENS Paris-Saclay, Université Sorbonne Paris Nord, Université Paris-Saclay,94235 Cachan, France, charyar.souzani@ens-paris-saclay.fr, nabil.anwer@ens-paris-saclay.fr, zzhu@ens-paris-saclay.fr, na.cai@ens-paris-saclay.fr
[2]Laboratoire Commun de Métrologie (LCM) Laboratoire National de Métrologie et d'Essais(LNE) 75015 Paris, France, yassir.arezki@lne.fr hichem.nouira@lne.fr

Corresponding author: Charyar Mehdi-Souzani, charyar.souzani@ens-paris-saclay.fr

Abstract. Multi sensor data fusion is a new challenge in dimensional metrology of freeform surfaces. Although data fusion processes have been extensively investigated in the literature and multi-sensor integrated systems are gradually being implemented by industry, the data obtained by the various sensors are not being optimally processed to assess the geometrical defects of complex workpieces. The work presented in this paper aims to propose a novel framework for form error assessment in multi sensor dimensional metrology. A generic and global approach in multi-sensor metrology combining registration, data fusion and fitting is proposed for aspherical and freeform optics. Driven by a curvature-based approach, the registration of data sets obtained from different sensors is conducted through a developed coarse and fine registration method. In order to improve the accuracy of the form error assessment for freeform surfaces, a data fusion-based method is proposed in this paper. A Gaussian Process (GP) model is built based on each of the transformed data sets, followed by the maximum likelihood data fusion. The fused result has improved characteristics and reduced uncertainty than either of the measurement data sets. Finally, a fitting algorithm is applied on the fused data for assessment of the minimum zone. To demonstrate the feasibility of the proposed method, simulation data and measurement data of aspheric optics are used and evaluated through case studies.

Keywords: data fusion; minimum zone; fitting; aspheric optics.
DOI: https://doi.org/10.14733/cadaps.2021.309-327

1 INTRODUCTION

Compared with traditional optic elements in spherical shape, aspheric and freeform optics have many advantages such as compactness and elimination of spherical aberration. Therefore, they

have replaced spherical elements in multiple optical systems and have been applied in different fields like medical imaging, astronomy, etc. [1-2].

Nowadays, the measurement of freeform surfaces is usually conducted with multiple sensors and requires the combination of different data processing techniques such as registration, data fusion and fitting.

Form errors evaluation is the main concern in terms of the performance of aspheric and freeform optical elements, so it is of great importance to assess the form deviations during the design and manufacturing. The assessed form deviations should always conform to tolerance specifications. One quality indicator of the form deviation is the Peak to Valley (PV). The least value of PV is referred as the Minimum Zone (MZ). However, the minimum zone evaluation can be affected by the measurement noise.

1.1   Related Work

Registration is essentially conducted in two steps [3] namely coarse and fine registrations. The coarse registration roughly aligns the two data sets from a global view. The resulting alignment is consequently optimized in the fine registration step to minimize a quadratic error.

In dimensional metrology, there is no standard coarse registration technique. As a promising method for coarse registration, Hough Transform (HT) was first attempted by [4] where only translations of the target object were considered. More recently, [5] extended the HT approach by including rotations and scale changes for the detection of non-parametric curves. The main concern of the HT algorithm is its complexity, which proportionally increases with the data volume since HT is based on an exhaustive search.

Fine registration refers to the set of techniques that obtain the Euclidean rigid motion between two or more data sets through iterative minimization. The commonly used fine registration methods are Iterative Closest Point (ICP) algorithm and its variants [6], which have been largely investigated regarding improvements in their speed, convergence and robustness. A classification and comparison of ICP variants is described in [7]. ICP algorithms operate in two steps: search for correspondences between points and computation of the Motion R (Rotation) and T (Translation). The main drawback of these techniques is the necessity to specify an initial guess to start the process which is expected to be quite close to the solution to guarantee the convergence. Hence, a good initial estimate of the transformation is required from the coarse registration.

For decades, considerable research attention has been paid to the fundamental problem of fitting models to a number of observations [8]. The evaluation of geometric deviations in coordinate metrology involves a minimization step in which a substitute surface should be fitted to the measured points. The choice of objective function and distance measure, which is used in fitting the substitute surface, has an effect on the estimation accuracy of geometric deviations to a certain extent. One of the most popular methods for smoothing random errors is to use the Lp-norms. Similarly, in coordinate metrology, the error objective function is defined by the Lp fitting norm. Three well-known types of Lp norms exist in literature, which could be applied for fitting purposes, namely L1-norm, L2-norm and L∞-norm. L2-norm is very popular and received a lot of interest by industry for its ease of implementation while overestimating form errors assessment. L∞-norm enables the computation of the least value PV and is recommended by actual ISO standards. However, the algorithmic issues are challenging in the context of freeform surfaces and large data sets.

Multi-sensor data fusion in dimensional metrology can be defined as the process of combining data from several information sources (sensors) into a common representational format in order that the metrological evaluation can benefit from all available sensor information and data [9-11]. There are various algorithms for data fusion. In this paper, we consider the most commonly used data fusion algorithms concerning dimensional metrology, namely the weighted least squares method, edge intensity method, Gaussian process model and Multilevel B-spline approximation.

Weighted least squares fusion is a fusion method based on parametric linear fitting of source surface data [12]. Forbes [13] developed a weighted least squares data fusion method based on Bayesian analysis of the measurement system. Ren et al. [14] developed a weighted least squares method for multi-sensor data fusion. Wang et al. [15] analyzed four types of weighted data fusion methods: least squares, pixel-levels, parametrical and non-parametrical methods. The advantage of weighted least squares fusion is its high computation speed. The difficulty lies in that it requires a good measurement model for accurate approximation of the source surface. Since weighted least squares fusion method relies on the fitting of source surface data, it is not applicable for complex geometries whose fitting solutions are not available or accurate.

Edge intensity data fusion method [16-17] involves decomposition of datasets into different regimes and fusion is carried out in each regime. Inverse transformation is performed on the fused datasets to obtain the final dataset. Ramasamy [18] proposed a Multi-Scale Data Fusion (MSDF) framework for surface metrology datasets. Coarse registration and fine registration are performed to align the datasets into the same coordinate system. Then the datasets are decomposed into three regimes which are form, waviness and roughness. In this way, data fusion is carried out on individual regimes based on the regional edge intensity method. Based on Ramasamy's work, Liu et al. [19] and Ren et al. [20] developed a multi-sensor data fusion method using Gaussian zero-order regression filter for decomposition and edge intensity method for fusion.

Gaussian process approximation is a non-parametric fitting method. Qian et al. [21] built a surrogate model based on Gaussian process model and adjusted it to a more accurate model using experimental results obtained from simulations. Later, this work was extended to the Bayesian hierarchical Gaussian process model for integration of low-accuracy and high-accuracy experiments. Xia et al. [22] built a Gaussian process model to assess the form errors using coordinate measurements. Later, using the similar method in Reference [23], Xia [24] developed a Bayesian hierarchical model which combines misaligned metrology data of two different resolutions to evaluate their geometrical quality. Colosimo et al. [25] proposed a two-stage Multi-sensor Data Fusion model (MsDF) using Gaussian process models for dimensional and geometric verification.

Despite the various research in this domain, a generic and global approach in multi-sensor metrology combining registration, data fusion and fitting has not been developed so far, in particular in the context of aspherical and freeform optics.

1.2 Proposed Method

The work presented in this paper aims to propose a novel framework for form error assessment in multi sensor dimensional metrology. A generic and global approach in multi-sensor metrology combining registration, data fusion and fitting is proposed for aspherical and freeform optics.

Driven by a curvature-based approach, the registration of data sets obtained from different sensors is conducted through a developed coarse and fine registration method. In order to improve the accuracy of the form error assessment for freeform surfaces, a data fusion-based method is proposed in this paper.

A Gaussian Process (GP) model is built based on each of the transformed data sets, followed by the maximum likelihood data fusion. The fused result has improved characteristics and reduced uncertainty than either of the measurement data sets. Finally, a fitting algorithm is applied on the fused data for assessment of the minimum zone. The general workflow of the proposed method is illustrated in Fig.1, from which it can be seen that registration, data fusion and fitting are the key methods.

In the following, research outcomes regarding the workflow process steps will be detailed and conclusions will be drawn. To demonstrate the feasibility of the proposed method, simulation data and measurement data of aspheric optics are used and evaluated through case studies.

The remainder of this paper is organized as follows: Section 2 presents the curvature-based registration method. In Section 3, the fitting method is explained for form error assessment.

Section 4 discusses the data fusion method integrating Gaussian Process models and maximum likelihood estimation. The proposed method is further tested on simulated data in Section 5. In Section 6, with a designed artefact, experimental validation is conducted based on measurement data and the results are discussed. Section 7 draws the conclusions.
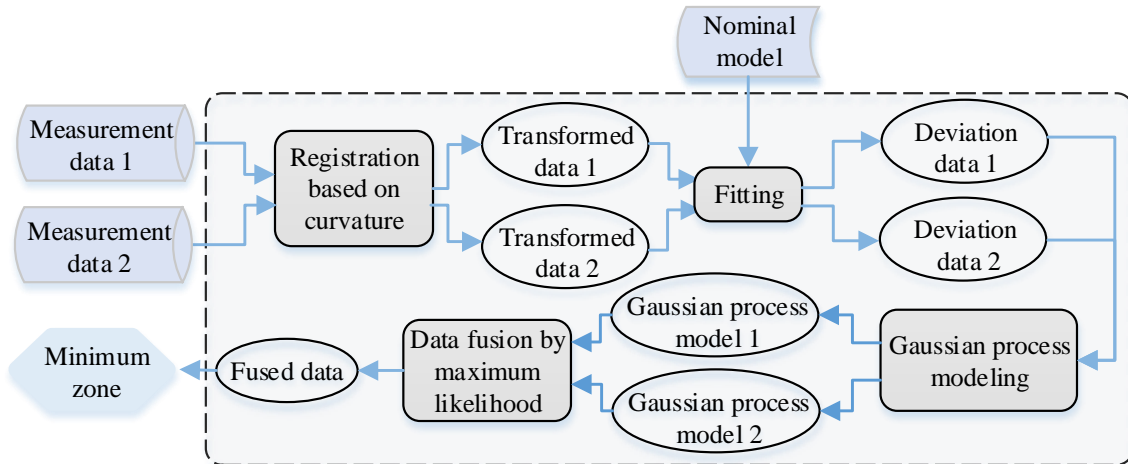

Figure 1: Illustration of the proposed method.

2   CURVATURE-BASED REGISTRATION

The registration process aims to determine the best alignment of two data types, Model data, (Q, the fixed set) and Scene data (P, the moving set) while combining them into the same coordinate system. In coarse registration, two measurement data sets in different coordinate systems are initially aligned in the same coordinate system. Then in fine registration, the matching vertex pairs in the two data sets are identified and the final registration parameters are obtained by minimizing the overall distance between these vertex pairs. In order to improve the efficiency and accuracy, curvature is used instead of the Euclidean distance to match vertices in both coarse registration and fine registration. The curvature-based registration is illustrated in Fig. 2.
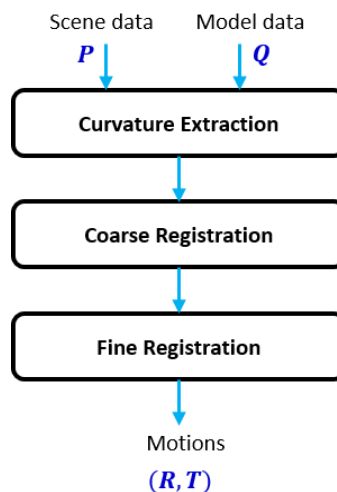

Figure 2: Curvature-based registration.

2.1   Curvature Definition and Calculation

Curvature is an important attribute that measures the shape of a surface. For a continuous smooth surface, the curvature is defined as the bending degree of a surface. Given a point P_i on the surface, for each unit direction $\vec{t}$ on its tangent plane, its normal curvature is defined as the curvature of the intersection curve of the surface and the perpendicular plane containing $\vec{t}$ and the normal direction of P_i. For discrete geometry, the curvature is calculated by the neighboring points. There are mainly three classes of discrete curvature approximation methods: one may approximate a local quadric surface on a given vertex to the meshes and then compute the derivatives to obtain the curvatures [26]; one may discretize the mathematical formulae of a smooth surface and extend it to discrete domains [27]; one may use the tensor based techniques for discrete curvature estimation [28] [29]. Thus, the last method is selected and applied here.

An additional weight coefficient λ_e has been introduced into the shape operator proposed by Cohen-Steiner and Morvan for discrete curvature estimation. The new shape operator $\boldsymbol{H}$ for a local region B around a vertex P becomes:

$$\boldsymbol{H} = \frac{1}{A}\sum_{e\in E}\lambda_e \cdot \beta(e)\cdot length\left(e\cap B\right)\cdot\left(\vec{e}\times\vec{e}\right) \tag{2.1}$$

$$\lambda_e = \frac{\cos^{-1}\left(\vec{\boldsymbol{n}}(\boldsymbol{p}),\vec{\boldsymbol{n}}(e)\right)}{\sum_{e\in E}\cos^{-1}\left(\vec{\boldsymbol{n}}(\boldsymbol{p}),\vec{\boldsymbol{n}}(e)\right)} \tag{2.2}$$

where, e is the edge of a triangle, $\vec{e}$ is a unit vector of e, $\vec{\boldsymbol{n}}(e)$ is the is the edge normal of the edge e, which is equal to the average normal vectors of the two triangles incident to the edge. $\beta(e)$ is the dihedral angle between the two normal vectors of the triangle incident with e, $\vec{\boldsymbol{n}}(\boldsymbol{p})$ is the normal of vertex P, B is the local region around vertex P, A is the area of B, E is the collection of all the mesh edges in B. The symbols and notations are described in the following figure (Fig.3).
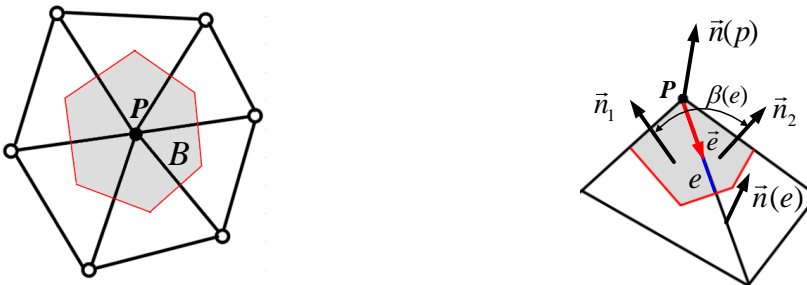

Figure 3: Tensor-based curvature estimation.

Two curvature attributes, shape index and curvedness, are used to describe the shape of a surface. The shape index (s) and curvedness (c) contain the local shape information equivalent to the pair of maximum and minimum curvatures or the pair of mean curvature and Gaussian curvature. Shape index specifies the shape type while curvedness specifies the size. They are both calculated based on the maximum principal curvature K_1 and the minimum principal curvature K_2, denoted as:

$$s = \frac{-2}{\pi} \arctan\left(\frac{K_1 + K_2}{K_1 - K_2}\right) \tag{2.3}$$

$$c = \frac{\sqrt{\left(K_1^2 + K_2^2\right)}}{2} \tag{2.4}$$

The local shapes to which a vertex belongs are classified into 10 types and visualized in specific colors, as shown in Table 1. Nine fundamental shape types can be identified according to the different intervals that the shape index falls in. The planar shape is identified when the curvedness is smaller than a given threshold C_p (C_p is a small value, e.g., C_p = 1x10^{-5}).

Shape Type	Identification	Shape type label	Color
Spherical cup	$s \in [-1, -7/8)$	-4	Green
Trough	$s \in [-7/8, -5/8)$	-3	Cyan
Rut	$s \in [-5/8, -3/8)$	-2	Blue
Saddle rut	$s \in [-3/8, -1/8)$	-1	Pale blue
Saddle	$s \in [-1/8, +1/8)$	0	White
Saddle ridge	$s \in [+1/8, +3/8)$	1	Pale yellow
Ridge	$s \in [+3/8, +5/8)$	2	Yellow
Dome	$s \in [+5/8, +7/8)$	3	Orange
Spherical cap	$s \in [+7/8, +1]$	4	Red
Plane	$c < c_p$	5	Black

Table 1: Shape types.

2.2 Coarse Registration Using Curvature-Based Hough Transformation Method

Since Hough transformation is based on an exhaustive search, the computational complexity increases with the data volume. Therefore, curvature is used for matching to reduce the number of iterations in the searching process.

For a pair of data sets to be registered: scene data P and model data Q, the local frames (V_i, V_j) should be built for all the vertices at first using the Eigen vectors obtained by eigen decomposition of the shape operator H. Then the possible transformation parameters for all the matching pairs between each vertex p_i in P and q_i in Q are calculated based on the local frames:

$$R_{i \to j} = V_j \cdot V_i^T \text{ and } T_{i \to j} = p_j - R_{i \to j} p_i \tag{2.5}$$

All the obtained transformation parameters are stored in the Hough table (HT) in ascending order according to the number of occurrences of each parameter. The best matching is achieved when the similarity between transformation parameters is sufficiently high:

$$dist\left(\left(R_{i\to j},T_{i\to j}\right)-\left(R,T\right)_{HT}\right)<\varepsilon_m \tag{2.6}$$

where ε_m is the residual less than 10^{-2}.

In the classic Hough transformation, all the local transformation parameters between each vertex p_i in P and q_i in Q need to be calculated, which leads to considerable computational cost. In order to improve the efficiency, curvature parameters are introduced to evaluate the degree of matching between the vertices first. The shape index and curvedness of all the vertices in both P and Q are calculated and the shape types of all the vertices can be identified. The vertices with the same shape types are matched initially and the transformation operations are only executed between these initially matching vertex pairs. In this way, the computational cost is decreased.

2.3 Fine Registration Using Curvature-Based ICP Method

The data sets are initially aligned in the same coordinate system and then fine registration is applied to all the vertices to determine the final registration parameters by minimizing the distance between two data sets. ICP is a common method used for registration, which mainly consists of two steps: matching and optimization.

The classical ICP method matches vertices according to their Euclidean distance. In this paper, a more comprehensive matching indicator d_m combining both Euclidean distance d_e and curvature distance d_c is used, which is calculated as:

$$d_m\left(p_i,q_i\right)=\lambda d_e+\left(1-\lambda\right)kd_c, k\in\mathbb{R}^{*+} \tag{2.7}$$

$$d_c=\sqrt{\left(\rho_{1p_i}-\rho_{1q_i}\right)^2+\left(\rho_{2p_i}-\rho_{2q_i}\right)^2} \tag{2.8}$$

$$d_e=\|p_i-q_i\| \tag{2.9}$$

$$\rho_1=\frac{1}{K_1},\ \rho_2=\frac{1}{K_2},\ \lambda\in[0,1]\ ,$$

where k is a constant to normalize d_c.

After matching the vertices, the transformation parameters (R,T) are calculated by solving a least square optimization problem. The objective function is defined with the combination of point-to-point (P-P) and point-to-plane (P-Pl) criteria and is formulated as:

$$\left(R,T\right)=\min_{R,T}\sum_{i=1}^{N_\Omega}w_i\left[\alpha_i\|Rp_i+T-q_i\|^2+\left(\beta_i\left(Rp_i+T-q_i\right)^Tn_i\right)^2\right] \tag{2.10}$$

where w_i is a weight indicating the reliable matching and its value is close to one. α_I and β_i are set according to the shape type of each vertex as shown in Table 2.

Shape type label	-4	-3	-2	-1	0	1	2	3	4	5
α_i	0.9	0.8	0.7	0.6	0.5	0.4	0.3	0.2	0.1	0
β_i	0.1	0.2	0.3	0.4	0.5	0.6	0.7	0.8	0.9	1

Table 2: The values of parameters α_I and β_i

3   FITING

After registration, the two measured data sets are transformed into the same coordinate system. Hence, fitting the data to the nominal shape is a crucial step in assessing the form error of the manufactured part.

Form error determination indicates the conformance of the manufactured shape to design tolerance specifications. For this purpose, a variability function must be defined. Among others, the Peak to Valley (PV), defined as the difference between maximum and minimum form deviations, is considered. The form deviation associated to the measured point P_i is its Euclidean distance to the nominal shape (Fig. 4).

P_i : A measured point
Q_i : Corresponding orthogonal projection
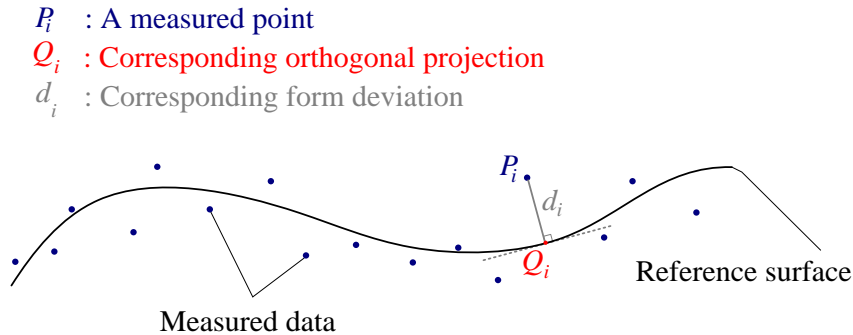d_i : Corresponding form deviation

Figure 4: Definition of form deviations.

The fitting procedure also requires the selection of an appropriate fitting criterion, where Least Squares and Chebyshev fitting are the most widely used. Each of these problems results in an optimisation problem with different mathematical properties. The PV returned by the Chebyshev fitting is the closest to the true value. However, this results in the optimization of a non-smooth objective function which is more difficult than LS fitting. The MZ fitting problem could be formulated as follows: Given a set of m measured data points $\{P_i\}_{1 \le i \le m}$ and their corresponding orthogonal projections $\{Q_i\}_{1 \le i \le m}$ onto a surface described using an implicit equation $f = (q, s)$ with $q = (x, y, z)$ as the coordinates of a given point on the surface and s as the surface' shape parameters. We aim at solving the problem given in (3.1).

$$\min_x \phi(x), \phi(x) = \max_{1 \le i \le m} f_i(x) \tag{3.1}$$

$f_i(x)$ denotes the Euclidean distance between the point P_i and its corresponding orthogonal projection Q_i. $x \in \mathbb{R}^n$ could be either the set of intrinsic shape parameters s or the motion parameters m : rotation and translation applied to $\{P_i\}$.

   This problem has been extensively investigated for simple geometries such as straightness, flatness, roundness and cylindricity [30], [31-32]. Nevertheless, this problem is still a relevant challenge for the case of freeform surfaces. Only few works were carried on in this area [33-34].

   In this work, the evaluation of the MZ value is conducted by means of an algorithm named the Hybrid Trust Region (HTR) algorithm [35]. This method consists of iteratively approximating the objective function given in (3.1) through quadratic programming and then using either trust region step, line search step or curve search step according to the actual situation at each iteration. In

this way, we avoid the repetitive resolution of the trust region problem. The numerical uncertainty associated to this problem on the returned minimum zone value is estimated as 10^{-15}mm.

4 DATA FUSION BASED ON GAUSSIAN PROCESS MODELING AND MAXIMUM LIKELIHOOD

After fitting, form deviations of the two data sets are obtained, on which data fusion is conducted in two steps. Both datasets contain the actual form deviations and the measurement noise, and their noise scale may also be different. The fusion process aims to effectively identify the actual form errors with reduced uncertainty and finally achieve a more reliable estimation of the minimum zone that is less sensitive to the noise. In the first step, the Gaussian process model with mean and uncertainty is built based on measured deviations of each transformed data set. Then the fused mean and uncertainty are estimated according to the maximum likelihood principle in the second step.

4.1 Gaussian Process Modeling of Measurement Data

Gaussian process has been proven to be an effective method to model the local random surface variation that exhibits the spatial distribution similarity [36]. The measurement data is the point cloud composed of vertices represented by their coordinates $(x_i, y_i, z_i)_{i=1,\cdots,n}$ and can be treated as the superposition of the true manufactured shape and the measurement error. The deviations of the measurement data from the nominal part shape can be extracted and represented in function form as:

$$\Delta z = f(x, y) + \varepsilon \tag{4.1}$$

where Δz is the measured deviations in Z-axis direction, $f(x, y)$ is the true form deviations in Z-axis direction, (x, y) is the input coordinate vector considered as the measured location, ε is the measurement error and it can be represented as an independent and identically distributed random variable at each location following a standard Gaussian distribution with zero mean and variance σ^2.

The true value $f(x, y)$ is unknown and the Gaussian process is used to estimate the $f(x, y)$ and its uncertainty as:

$$f(x, y) \sim GP\big(m(x, y), k\big((x, y),(x', y')\big)\big) \tag{4.2}$$

where $m(x, y)$ is the mean function at location (x, y) and $k\big((x, y),(x', y')\big)$ is the covariance function evaluated at location (x, y) and (x', y'). They can be calculated as (11) and (12), in which $E(\cdot)$ denotes the expectation operator.

$$m(x, y) = E\big[f(x, y)\big] \tag{4.3}$$

$$k\big((x, y),(x', y')\big) = E[(f(x, y) - m(x, y))(f(x', y') - m(x', y'))] \tag{4.4}$$

Once the Gaussian process model is built, any prediction f_p at new location (x_p, y_p) can be obtained by the joint distribution of the measured value in Z-axis direction and the function value at the prediction locations. The prediction equation is

$$f_p \big| (X,Y), z, (X_p, Y_p) \sim N\left(\overline{f}_p, \text{cov}\left(f_p\right)\right) \tag{4.5}$$

where

$$\overline{f}_p = E\left[f_p \big| (X,Y), z, \left(X_p, Y_p\right)\right] = K\left((X_p, Y_p),(X,Y)\right)\left[K\left((X,Y),(X,Y)\right)+\sigma^2 I\right]^{-1} z$$

$$\text{cov}\left(f_p\right) = K\left((X_p, Y_p),(X_p, Y_p)\right) - K\left((X_p, Y_p),(X,Y)\right)\left[K\left((X,Y),(X,Y)\right)+\sigma^2 I\right]^{-1} K\left((X,Y),(X_p, Y_p)\right)$$

$E(\cdot)$ and $K(\cdot,\cdot)$ share the same definition as in (4.3) and (4.4), (X,Y) is the matrix of the measured locations, (X_p, Y_p) is the matrix of locations at which the values are to be predicted, σ^2 is the measurement error variance and I is the identity matrix.

4.2 Data Fusion by Maximum Likelihood

By building the Gaussian process model for the two measured deviation datasets, we can estimate the mean and the uncertainty of any vertex in the point cloud. Considering two measurement datasets, we can evaluate the means and the uncertainties as m_1, m_2 and u_1, u_2, for the two datasets, respectively. Since the measurement noise is in Gaussian distribution, then the probability of both the two measurements getting result m can be calculated as

$$p\left(m\big| m_1, u_1^2\right) = \frac{1}{u_1\sqrt{2\pi}} e^{-\frac{(m-m_1)^2}{2u_1^2}} \tag{4.6}$$

$$p\left(m\big| m_2, u_2^2\right) = \frac{1}{u_2\sqrt{2\pi}} e^{-\frac{(m-m_2)^2}{2u_2^2}} \tag{4.7}$$

Then the likelihood of both two measurements getting m at specific position is

$$p\left(m\big| m_1, u_1^2, m_2, u_2^2\right) = p\left(m\big| m_1, u_1^2\right) p\left(m\big| m_2, u_2^2\right) = \frac{1}{2\pi u_1 u_2} e^{-\left[\frac{(m-m_1)^2}{2u_1^2} + \frac{(m-m_2)^2}{2u_2^2}\right]} \tag{4.8}$$

The corresponding natural logarithm is

$$\ln\left(p\left(m\big| m_1, u_1^2, m_2, u_2^2\right)\right) = -\left[\frac{(m-m_1)^2}{2u_1^2} + \frac{(m-m_2)^2}{2u_2^2}\right] + \ln\left(\frac{1}{2\pi u_1 u_2}\right) \tag{4.9}$$

Based on the maximum likelihood principle, we can obtain the best estimation of m by maximizing (4.9). Therefore, we calculate the partial derivative of (4.9) to m as

$$\frac{\partial \ln\left(p\left(m\big| m_1, u_1^2, m_2, u_2^2\right)\right)}{\partial m} = \frac{\partial\left\{-\left[\frac{(m-m_1)^2}{2u_1^2} + \frac{(m-m_2)^2}{2u_2^2}\right] + \ln\left(\frac{1}{2\pi u_1 u_2}\right)\right\}}{\partial m} \tag{4.10}$$

By solving (4.10), we can obtain the best estimated value

$$\overline{m} = \left(\frac{m_1}{u_1^2} + \frac{m_2}{u_2^2} \right) \bigg/ \left(\frac{1}{u_1^2} + \frac{1}{u_2^2} \right) \tag{4.11}$$

If we define two weights ω_1 and ω_2 as $\omega_1 = \dfrac{1}{u_1^2}$ and $\omega_2 = \dfrac{1}{u_2^2}$

Then (4.11) can be written as

$$\overline{m} = \frac{\omega_1 m_1 + \omega_2 m_2}{\omega_1 + \omega_2} \tag{4.12}$$

The uncertainty of $\overline{m}$ can be calculated according to the uncertainty propagation principle as:

$$\overline{u} = \sqrt{\left(\frac{\omega_1}{\omega_1 + \omega_2} u_1 \right)^2 + \left(\frac{\omega_2}{\omega_1 + \omega_2} u_2 \right)^2} = \frac{1}{\sqrt{\omega_1 + \omega_2}} \tag{21}$$

It can be seen that the uncertainty after maximum likelihood fusion is smaller than any of two measurement datasets.

5   TESTING ON SIMULATED DATA

The simulation is conducted on an aspheric optical part whose shape is generated with certain control parameters. The mathematical form of an aspherical shape is defined following the equation specified in ISO 1110-12:

$$z(r) = \frac{r^2}{R\left(1 + \sqrt{1 - (1+\kappa)r^2 / R^2}\right)} + \alpha_4 r^4 + \alpha_6 r^6 + \alpha_8 r^8 + \ldots \tag{5.1}$$

where $z(r)$ is the sag at distance $r = \sqrt{x^2 + y^2}$ from the central axis, α_i are coefficients that measure the surface deviation from the axially symmetric quadric surface defined by R and κ. A set of 5025 grid points are sampled in the 2D space and their coordinates (x, y) are used to calculate the values of r. Hence, the nominal shape of the part is generated by setting the parameters as:

$$R = 9.1276 \ 10^{+10}, \ \kappa = -1, \ a_4 = 1.2783 \ 10^{-5},$$
$$a_6 = 7.9222 \ 10^{-10}, \ a_8 = -1.8598 \ 10^{-11}, \ a_{10} = -1.8598 \ 10^{-15}$$

The actual form deviations are generated following a predefined mathematical equation given as: $f(x, y) = \cos(0.0025x) + \cos(0.0025y)$. Figure 5 illustrates the generated nominal part surface as well as the simulated form deviations.

To account for the measurement errors, noise is added to the simulated form deviations, as shown in Figure 5(b). To emphasize the discrepancies between the two measurement datasets, their noise scales are specified differently. The noise is generated with zero-mean Gaussian distribution $\varepsilon(x, y) \sim N(0, \sigma^2)$ at (x, y) locations.
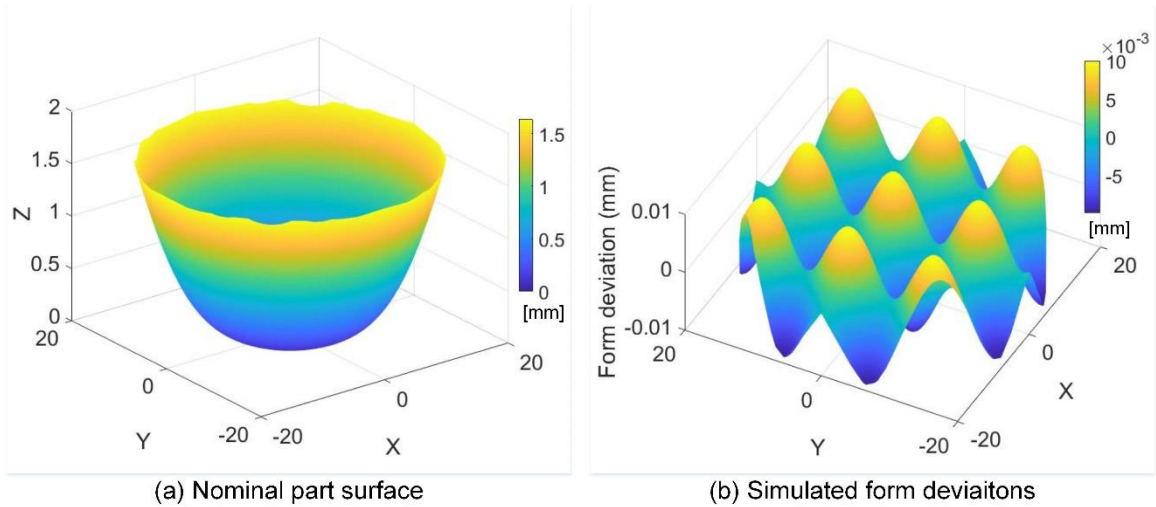
(a) Nominal part surface   (b) Simulated form deviaitons

Figure 5: The nominal surface and form deviations of the simulated part.

For one dataset, the noise is generated at ∼500 points randomly sampled from the 5000 points with $\sigma_1 = 0.0002\text{mm}$. This dataset is intended to imitate data collected from a tactile probe, which has better accuracy but with a number of sample points which is comparatively lower. For the other dataset, the noise is generated for all the 5000 points with $\sigma_2 = 0.002mm$, imitating data from a scanning device which has lower accuracy. The resulting distribution of coupled form deviations and measurement errors of both datasets can be visualized in Figure 6(a) and (b).

The Gaussian Process model of both datasets are derived based on the simulated datasets $(x, y, \Delta z)$, where $\Delta z = f(x, y) + \varepsilon(x, y)$ denotes the simulated form deviations superposed with the generated noise. The GP models are further used to make predictions on all the data points. Figure 7 shows the mean prediction and prediction interval of the GP model for measurement data 1. It can be seen that the mean prediction reaches a close fitting to the real form deviations after training with the noisy data, and the 95% prediction interval almost fully encloses the noise, indicating the accurate capture of the uncertainty. The average range of the prediction interval is $\sigma_1 = 0.0078\text{mm}$. Similarly, the results of measurement data 2 are illustrated in Figure 8. With a subset of only 10% of the training data points as used in measurement data 1, the GP model realizes an accurate prediction on all the other points. Since the noise scale used for this dataset is smaller, the prediction interval is narrower compared with dataset 1, reaching an average range of $\sigma_2 = 9.1131 0^{-4}\text{mm}$.

Data fusion is then conducted based on the mean and variance predicted by the two GP models at each point. The mean prediction and prediction interval of the fused model is shown in Figure 9. After data fusion, the average range of the interval falls to $\sigma_{fuse} = 7.3125 10^{-4}mm$, which is smaller than both σ_1 and σ_2 before fusion. It can be concluded that, through GP modeling, the actual form deviations can be captured among the measurement noise, even with a small number of sample points. Through data fusion, the uncertainty of both GP models, as interpreted by the range of prediction interval, is reduced, which facilitates filtering out the noise in data and the robust assessment of the form deviations.
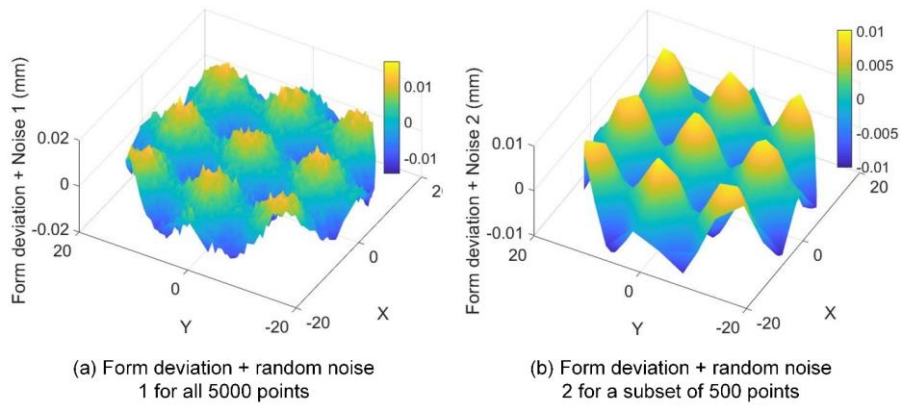
(a) Form deviation + random noise
1 for all 5000 points

(b) Form deviation + random noise
2 for a subset of 500 points

Figure 6: Form deviation and generated noise for two simulated measurement datasets.

(a) Mean GP prediction of
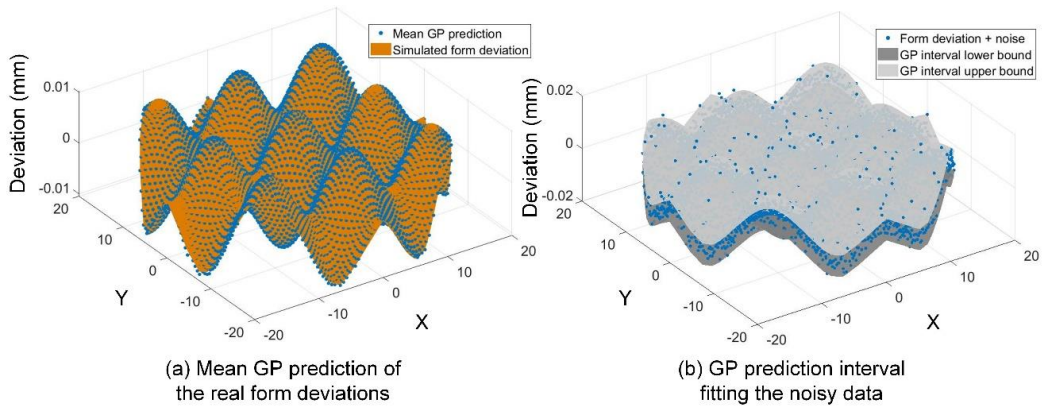the real form deviations

(b) GP prediction interval
fitting the noisy data

Figure 7: Mean prediction and prediction interval of the GP model for measurement data 1.

(a) Mean GP prediction of
the real form deviations

(b) GP prediction interval
fitting the noisy data
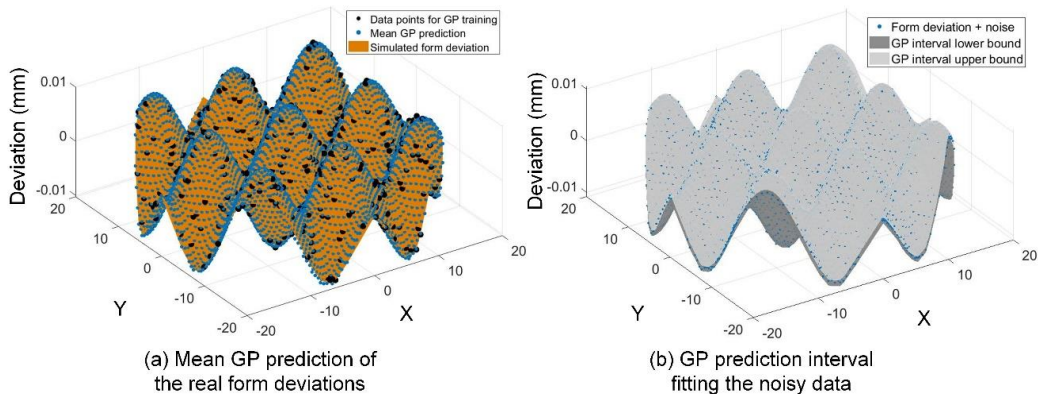
Figure 8: Mean prediction and prediction interval of the GP model for measurement data 2.

(a) Prediction of form deviation after data fusion

(b) Prediction interval after data fusion
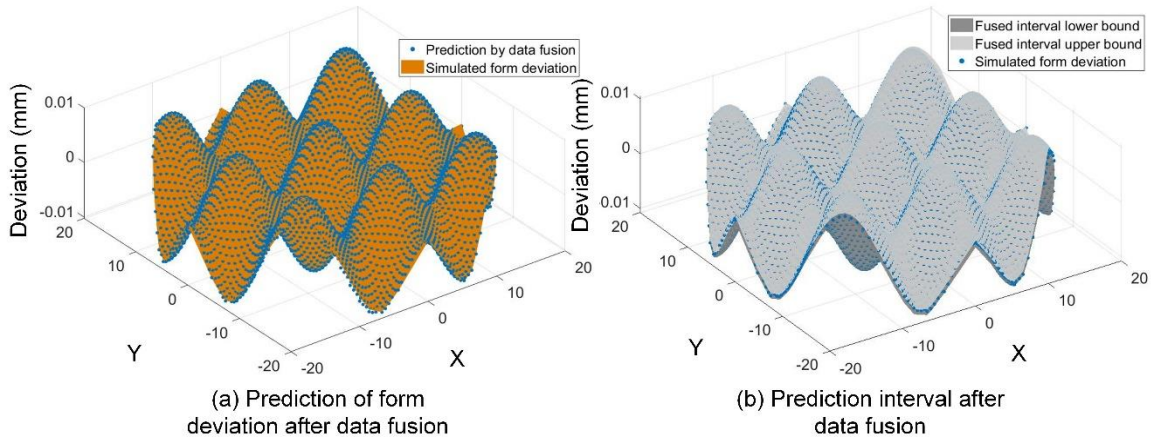
Figure 9: Mean prediction and prediction interval of the data fusion model.

6   TESTING ON MEASURED DATA

The proposed data fusion method is then tested on two measurement datasets obtained by the mean of the measurement of a manufactured aspherical part described using the ISO10110-12 formulation. The nominal shape coefficients are given as follow: R=31.075, k=-0.744, a4=4.36 $\times 10^{-7}$, a6=-2.27 $\times 10^{-10}$, a8=-1.70 $\times 10^{-13}$, a10=-3.68 $\times 10^{-17}$, a12=8.94 $\times 10^{-22}$, a14=1.85 $\times 10^{-23}$ and A16=-6.27 $\times 10^{-27}$. Measurements were conducted using LuphoScan 260 HD (measurement 1) and MarForm MFU 200 Aspheric 3D (measurement II). Measurement data 1 contains a total number of 612 points measured from the surface, while the point density in measurement data 2 is much higher, resulting in 73228 points. In the first step, curvature-based registration is conducted to transform both datasets into a common coordinate system. The transformed datasets are illustrated in Figure 10. Based on the known nominal shape of the artefact, the deviations of measurement data are obtained through the fitting approach and denoted as $(x,y, \Delta z)$. The obtained deviations comprise both the actual form deviations and noise introduced due to measurement errors, as shown in Figure 11. The objective is to use the GP model and data fusion to have an accurate estimation of the actual form deviations with reduced uncertainty, which can be further used to derive the optimized assessment of minimum zone for this free-form artefact.

The GP models of both deviation datasets are trained with (x,y) as input variables and Δz as the response variable. The mean prediction and 95% prediction interval of the trained GP models are illustrated with respect to the training data in Figure 12 and Figure 13 respectively. Note that the 95% prediction interval is considered as a zone that encloses most of the measured data points. The minimum zone can be derived by evaluating the largest absolute deviation of the prediction interval from the mean prediction and offsetting the mean prediction along the positive and negative Z direction with this value. According to this definition, the minimum zone is $MZ_1 = 3.68622\ 10^{-5}\ mm$ and $MZ_2 = 4.7277\ 10^{-5}\ mm$ for measurement data 1 and 2 respectively.
Performing data fusion based on the GP models, a final estimation of the form deviations and the minimum zone can be achieved. Figure 14(a) shows the estimation result compared with the measured deviation datasets. The fused model enables to identify a more realistic distribution of the form deviations on the surface among the two noisy data. Moreover, from the uncertainty interval illustrated in Figure 14(b), the minimum zone of the fused model is derived as $MZ_{fuse} = 2.1079\ 10^{-5}\ mm$, which is significantly reduced compared with those derived from the single GP models before fusion. Therefore, the effectiveness of the data fusion method in form deviation and minimum zone assessment is justified.
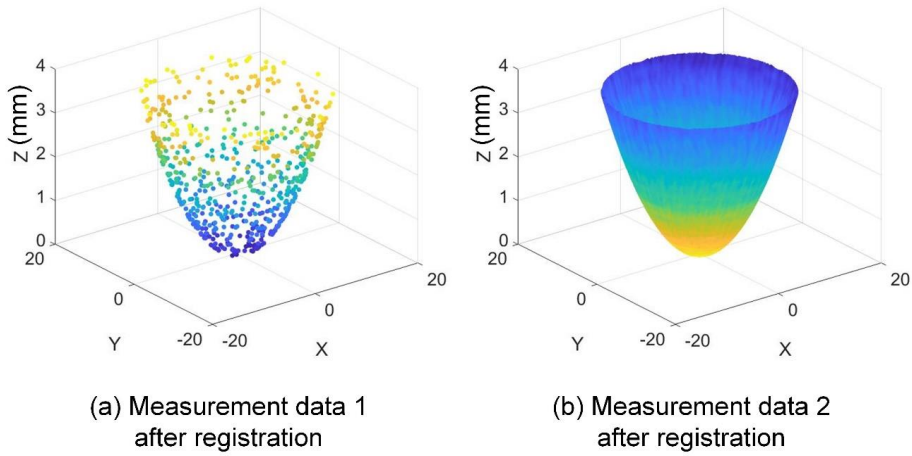
(a) Measurement data 1
after registration

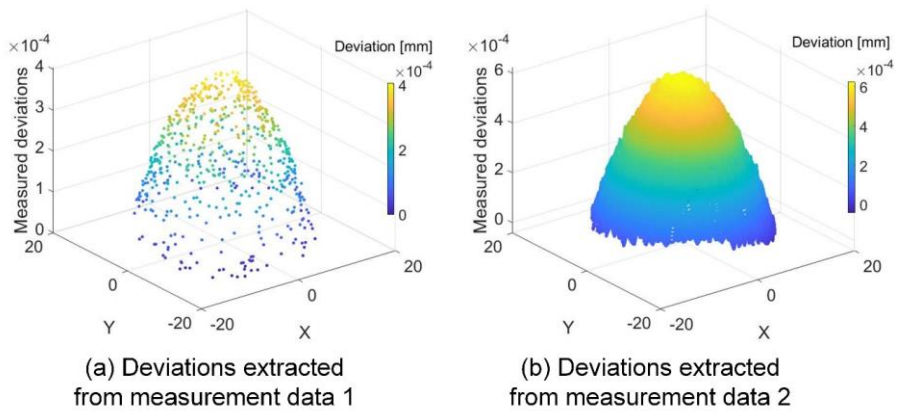(b) Measurement data 2
after registration

Figure 10: Measurement datasets after registration.

(a) Deviations extracted
from measurement data 1

(b) Deviations extracted
from measurement data 2

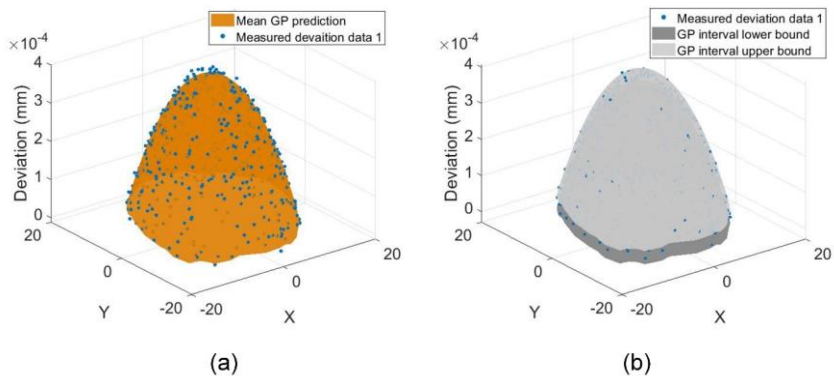**Figure 11**: Deviations extracted from the registered measurement data.

(a)

(b)

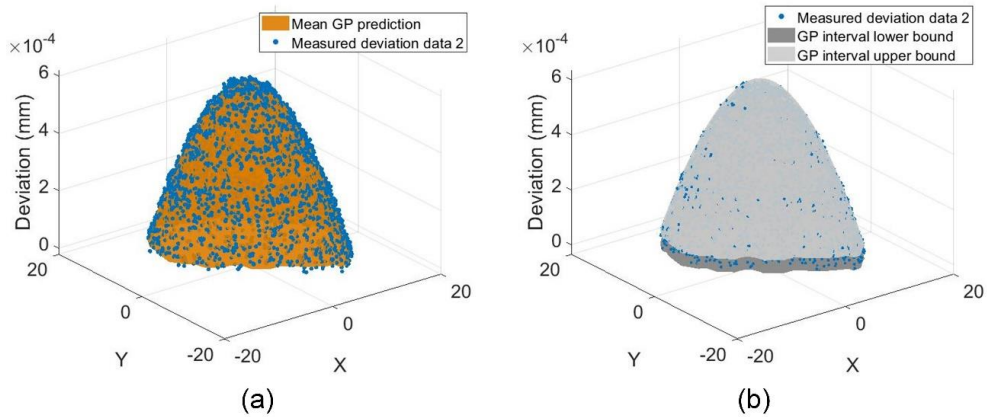**Figure 12**: GP modeling result for measured deviation data 1.

Figure 13: GP modeling result for measured deviation data 2.

(a) Estimated form deviations compared with two measured datasets

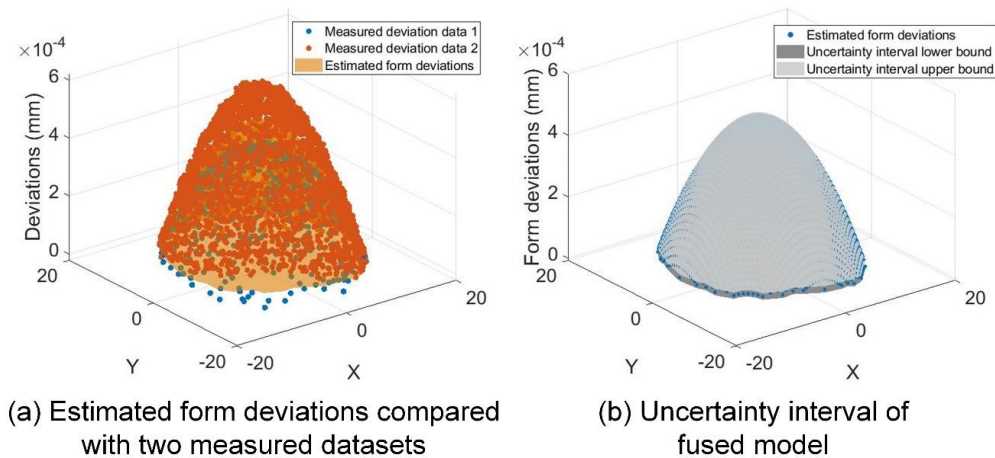(b) Uncertainty interval of fused model

Figure 14: Data fusion result.

7   CONCLUSION

Aspheric optical elements have many advantages compared to regular spherical lenses. However, those advantages are closely linked to their geometry quality in term of form deviation. Thus, an accurate measurement of the form deviation of aspheric and freeform optic parts is highly required. Furthermore, it must be taken into account that the measurement of aspheric and free form optic parts generally requires the use of multiple sensors. So one can collect several clouds of points with various characteristics. As a consequence, data processing is a major source of potential error in the process of measurement. Data processing becomes more complex and a crucial step to the assessment of the form deviation.

A review of literature shows that multi-sensor data fusion has been investigated nevertheless most of the developed methods and algorithms failed when they are applied to aspherical and freeform optics. Thus, in this paper we have introduced a generic and global approach for data treatment of multi-sensor metrology combining three steps: registration, fitting and data fusion. Furthermore, the developed method takes into account the specific characteristics of aspherical

surface. The novel framework introduced is based on the Peak to Valley quality indicator for the form deviation assessment and start with a registration step based on curvature computation. Then we have introduced a min-max fitting method for form error assessment and finally a data fusion method integrating Gaussian Process models and maximum likelihood estimation. The feasibility of the developed framework was demonstrated through simulation data and also real measurement data of a designed artefact.

8   ACKNOWLEDGMENT

Zuowei Zhu, http://orcid.org/0000-0002-9688-8176
Na Cai, http://orcid.org/0000-0003-2322-2653
Charyar Mehdi-Souzani, http://orcid.org/0000-0003-3049-2176
Nabil Anwer, http://orcid.org/0000-0002-0771-4685

REFERENCES

[1]   Geary, J. M.: Introduction to Lens Design: With Practical ZEMAX Examples, Willmann-Bell, Richmond, VA, 2002.
[2]   Karow, H. K.: Fabrication Methods for Precision Optics, Wiley, New York, NY, 2004.
[3]   Kim, T.; Seo, Y.; Lee, S.: Simultaneous registration of multiple views with markers, Journal of Computer-Aided Design, 41(4), 2009, 231-239. https://doi.org/10.1016/j.cad.2008.10.007
[4]   Merlin, P. M.; Farber, D. J.: A parallel mechanism for detecting curves in pictures, IEEE Transactions on Computers, 100(1), 1975, 96–98. https://doi.org/10.1109/T-C.1975.224087
[5]   Ballard, D. H.: Generalizing the Hough Transform to detect arbitrary shapes, Pattern Recognition, 13(2), 1981, 111–122. https://doi.org/10.1016/0031-3203(81)90009-1
[6]   Besl, P.; McKay, N.: A method for registration of 3D shapes, Transactions of IEEE on PAMI, 14(2), 1992, 239-56. https://doi.org/10.1117/12.57955
[7]   Tam, G. K.; Cheng, Z.-Q.; Lai, Y.-K.; Langbein, F. C.; Liu, Y.; Marshall, D.; Martin, R. R.; Sun, X.-F.; Rosin, P. L.: Registration of 3D point clouds and meshes: a survey from rigid to nonrigid, IEEE Transactions on Visualization and Computer Graphics, 19(7), 2013, 1199-1217. https://doi.org/10.1109/TVCG.2012.310
[8]   Gonin, R.; Money, A. H.: Nonlinear Lp-Norm Estimation, Routledge, New York, NY, 1989.
[9]   Liggins, M.; Hall, D.; Llinas, J.: Handbook of Multisensor Data Fusion: Theory and Practice, Second Edition, CRC Press, Boca Raton, FL, 2017.
[10] Colosimo, B. M; Senin, N.: Geometric tolerances: impact on design, inspection and process monitoring, Springer, London, 2010.
[11] Shen, T.-S.; Huang J.-B.; Menq, C.-H.: Multiple-sensor integration for rapid and high-precision coordinate metrology, IEEE/ASME Transactions on Mechatronics, 5, 2000, 110–21. https://doi.org/10.1109/3516.847084
[12] Strutz, T.: Data fitting and uncertainty: a practical introduction to weighted least squares and beyond, Vieweg and Teubner, Germany, 2010.
[13] Forbes, A. B.: Weighting observations from multi-sensor coordinate measuring systems, Measurement Science and Technology, 23(2), 2012, 025004.
[14] Ren, M. J.; Sun, L. J.; Liu, M. Y.; Cheung, C. F.; Yin, Y. H.; Cao, Y. L.: A weighted least square based data fusion method for precision measurement of freeform surfaces, Precision Engineering, 48, 2017, 144-151. https://doi.org/10.1016/j.precisioneng.2016.11.014

[15] Wang J.; Pagani L.; Leach R. K.; Zeng, W.; Colosimo, B. M.; Zhou, L.: Study of weighted fusion methods for the measurement of surface geometry, Precision Engineering, 47. 2017, 111-121. https://doi.org/10.1016/j.precisioneng.2016.07.012

[16] Ramasamy, S. K.: Multi-Scale Data Fusion for Surface Metrology, Ph.D. thesis, University of North Carolina at Charlotte, Charlotte, NC, 2011.

[17] Ramasamy, S. K.; Raja, J.; Boudreau, B. D.: Multi-Sensor Data Fusion in Surface and Dimensional Metrology Domains, Proceedings of 40th North American Manufacturing Research Conference, University of Notre Dame, Indiana, IN, 2012.

[18] Ramasamy, S. K.; Raja, J., Boudreau, B. D.: Data fusion strategy for multiscale surface measurements, Journal of Micro and Nano-Manufacturing, 1(1), 2013, 011004. https://doi: 10.1115/1.4023755

[19] Liu, M.-Y.; Cheung, C.-F., Ren, M.-J.: A Framework of Data Fusion Algorithm for Precision Measurement of Multiscale Surfaces, Key Engineering Materials, 679, 2016, 155-161. https://doi.org/10.4028/www.scientific.net/KEM.679.155

[20] Ren, M.-J.; Liu, M.-Y.; Cheung, C.-F.: Multi-sensor data fusion for measurement of complex freeform surfaces, Seventh International Symposium on Precision Mechanical Measurements, International Society for Optics and Photonics, 9903, 2016, 990316. https://doi.org/10.1117/12.2211638

[21] Qian, Z.; Seepersad, C. C.; Joseph, V. R.; Allen, J. K.; Wu, C. J.: Building surrogate models based on detailed and approximate simulations, Journal of Mechanical Design, 128(4), 2006, 668-677.

[22] Xia, H.; Ding, Y.; Wang, J.: Gaussian process method for form error assessment using coordinate measurements, IIE Transactions, 40(10), 2008, 931–946. https://doi.org/10.1080/07408170801971502

[23] Qian, P. Z.; Wu, C. J.: Bayesian hierarchical modeling for integrating low-accuracy and high-accuracy experiments, Technometrics, 50(2), 2008, 192-204, https://doi.org/10.1198/004017008000000082

[24] Xia, H.; Ding, Y.; Mallick, B. K.: Bayesian hierarchical model for combining misaligned two-resolution metrology data, IIE Transactions, 43(4), 2011, 242-58, https://doi.org/10.1080/0740817X.2010.521804

[25] Colosimo, B. M.; Pacella, M.; Senin, N.: Multisensor data fusion via Gaussian process models for dimensional and geometric verification, Precision Engineering, 40, 2015, 199-213. https://doi.org/10.1016/j.precisioneng.2014.11.011

[26] Khameneifar, F.; Ghorbani, H: On the curvature estimation for noisy point cloud data via local quadric surface fitting, Computer-Aided Design & Applications, 16(1), 2019, 140-149. https://doi.org/10.14733/cadaps.2019.140-149

[27] Meyer, M.; Desbrun, M.; Schröder, P.; Barr, A. H.: Discrete differential-geometry operators for triangulated 2-manifolds, Visualization and mathematics III, Springer, Berlin, Heidelberg, 2003.

[28] Cohen-Steiner, D.; Morvan, J. M.: Restricted delaunay triangulations and normal cycle, Proceedings of the nineteenth annual symposium on Computational geometry, 2003, 312-321.

[29] Taubin, G.: Estimating the tensor of curvature of a surface from a polyhedral approximation. Proceedings of IEEE International Conference on Computer Vision, 1995, 902-907, https://doi.org/10.1109/ICCV.1995.466840

[30] Murthy, T. S. R.; Abdin, S. Z.: Minimum zone evaluation of surfaces, International Journal of Machine Tool Design and Research, 20(2), 1980, 123-136. https://doi.org/10.1016/0020-7357(80)90024-4

[31] Samuel, G. L.; Shunmugam, M. S.: Evaluation of straightness and flatness error using computational geometric techniques, Computer-Aided Design, 31(13), 1999, 829-843. https://doi.org/10.1016/S0010-4485(99)00071-8

[32] Huang, S.-T.; Fan, K.-C.; Wu, J.-H.: A new minimum zone method for evaluating flatness errors, Precision engineering, 15(1), 1993, 25-32. https://doi.org/10.1016/0141-6359(93)90275-F

[33] Zhang, X.; Zhang, H.; He, X.; Xu, M.; Jiang, X.: Chebyshev fitting of complex surfaces for precision metrology, Measurement, 46(9), 2013, 3720-3724. https://doi.org/10.1016/j.measurement.2013.04.017

[34] Zhang, X.; Jiang, X.; Forbes, A. B.; Minh, H. D.; Scott, P. J.: Evaluating the form errors of spheres, cylinders and cones using the primal–dual interior point methods, Proceedings of the Institution of Mechanical Engineers, Part B: Journal of Engineering Manufacture, 227(5), 2013, 720-725. https://doi.org/10.1177/0954405413476494

[35] Arezki, Y.; Nouira, H.; Anwer, N.; Mehdi-Souzani, C.: A novel hybrid trust region minimax fitting algorithm for accurate dimensional metrology of aspherical shapes, Measurement, 127, 2018, 134-140. https://doi.org/10.1016/j.measurement.2018.05.071

[36] Shao, C.; Ren, J.; Wang, H.; Jin, J.-J.; Hu, S.-J.: Improving machined surface shape prediction by integrating multi-task learning with cutting force variation modeling, Journal of Manufacturing Science and Engineering, 139(1), 2017, 011014. https://doi.org/10.1115/1.4034592